RSC Advances

PAPER

View Article Online
View Journal | View Issue

Cite this: *RSC Adv.*, 2018, **8**, 20354

Photo-reduction of heavy metal ions and photo-disinfection of pathogenic bacteria under simulated solar light using photosensitized TiO_2 nanofibers†

Samina Ghafoor,[ab] Syed Zajif Hussain,[a] Sadia Waseem[b] and Salman Noshear Arshad *[a]

We report the photosensitization of electrospun titania nanofibers, with a mean diameter of 195 nm, by low bandgap silver sulfide nanoparticles of 11–23 nm mean size with the aim of treating heavy metal ions and pathogenic bacteria simultaneously under simulated solar light irradiation. The 17 nm Ag_2S/TiO_2 nanofibers showed 90% photocatalytic reduction of Cr(VI) at pH of 3 with a pseudo-first order rate constant of 0.016 min^{-1} which is significantly better than the previously reported for Ag–Ag_2S/TiO_2 composite particles. The antibacterial capability of the Ag_2S/TiO_2 nanofibers was evaluated *via* photo-disinfection of the Gram-positive and Gram-negative bacterial strains. The smallest sized 11 nm Ag_2S/TiO_2 nanofiber showed the best bactericidal efficiency of 100% and 90.6% against Gram-negative *E. coli* and Gram-positive *S. aureus* after 1 h of irradiation, respectively, whereas, only 50% *E. coli* and 41% *S. aureus* were found to be inactivated in dark. Furthermore, a UV–O_3 treatment of the 11 nm Ag_2S/TiO_2 nanofibers remarkably enhanced the antibacterial activity where 89% *E. coli* and 81% *S. aureus* were inactivated in just 10 min of the irradiation. Enhanced photocatalytic activity is attributed to the efficient charge separation and transfer and reduced electron–hole recombination induced by the effective heterojunction formation between TiO_2 and the optimally sized Ag_2S nanoparticles. The disinfection nature of the Ag_2S nanoparticles, role of the generated hydroxyl species under irradiation, and the cell wall damage mechanism is also discussed. This study demonstrates the potential use of these multifunctional composite TiO_2 nanofibers for water remediation.

Received 8th February 2018
Accepted 29th May 2018

DOI: 10.1039/c8ra01237g

rsc.li/rsc-advances

Introduction

Degradation of water quality by harmful organic and inorganic pollutants is a serious problem world-wide leading to millions of deaths annually.[1,2] Pathogenic micro-organisms cause water-borne diseases such as diarrhea, cholera, gastroenteritis, *etc.* which may be fatal.[3] There are several disinfectants used commonly for the effective control of pathogens in drinking water such as free chlorine, chloramines and ozone, *etc.* However, these usually result in the formation of the harmful disinfection by-products (DBPs), many of which are carcinogenic.[4] Thus, there is a dire need to develop new green technologies of disinfection which are efficient, low cost, sustainable and environmentally friendly.

Moreover, contamination of water by heavy metals is another health risk because they have a tendency to store and accumulate in the living organisms causing several diseases and disorders.[5] For example, hexavalent chromium, Cr(VI), is one of the most common inorganic water pollutants originating from the industries such as electroplating, leather tanning, and textile, *etc.*[6,7] Most of the Cr(VI) compounds have proven to be toxic, carcinogenic and mutagenic.[8] However, trivalent chromium, Cr(III), is less toxic and less mobile in nature as compared to the Cr(VI) and can be easily removed in the form of hydroxides. To this end, numerous catalysts are being reported for the conversion of Cr(VI) to Cr(III) state.[9–13]

Recently, the increasing demand of industrial wastewater treatment and focus on solar energy conversion has renewed interest in developing novel heterogeneous photocatalysis based water remediation technologies. For example, photo-degradation using suitable bandgap semiconductor materials has been extensively investigated as an effective and energy efficient strategy for the eradication of hazardous pollutants from the wastewater.[14–16] Since the discovery of the photo-catalytic activity of titanium dioxide (TiO_2) by Fujishima and

[a]*Department of Chemistry and Chemical Engineering, Syed Babar Ali School of Science and Engineering, Lahore University of Management Sciences, Lahore 54792, Pakistan. E-mail: salman.arshad@lums.edu.pk*

[b]*Institute of Chemistry, University of the Punjab, P. O. Box 54590, Lahore, Pakistan*

† Electronic supplementary information (ESI) available. See DOI: 10.1039/c8ra01237g

Honda in 1972,[17] it has been widely studied due to its preferred band positions, high photocatalytic activity, high resistance to corrosion, low cost, and lack of toxicity.[18] However, the limited light absorbance in the visible range of the solar spectrum and the fast electron–hole recombination kinetics are the two major hurdles for its practical applications.

To address these challenges, several attempts have been made such as coupling TiO_2 with narrow bandgap semiconductors,[19,20] metal and non-metal doping,[21–23] dye sensitization,[24,25] and surface modification with noble metals.[26] Metal oxides and sulfides have drawn great attention as both core photocatalyst as well as co-catalyst.[27,28] Among metal sulfides, silver sulfide (Ag_2S) is considered a potential candidate for the photosensitization of TiO_2 because of its low bandgap ($E_g \sim 1.0$ eV) and desired band positions relative to TiO_2, making it active in the visible range of the solar spectrum.[29] Moreover, due to its photocatalytic activity and ability to develop strong oxidizing power when irradiated under UV light, TiO_2 shows noticeable antibacterial effect which can be further enhanced by doping or heterojunction formation.[30–34]

Silver and silver-based nanomaterials are well-known potential antimicrobial agents owing to their high cytotoxicity for microorganisms and outstanding broad-spectrum antimicrobial activity against different strains of the bacteria.[35–38] Pang *et al.*[39] explored the antibacterial properties of Ag_2S/Ag heterodimers against *E. coli*. Zhang *et al.*[40] synthesized hollow spherical Ag–Ag_2S/TiO_2 nanocomposites for the photo-reduction of Cr(VI) under UV-visible irradiation. Size and shape of the nanoparticles (NPs) significantly affect their photocatalytic and antibacterial activity.[41] A comparative study of the antibacterial properties of spherical, triangular and rod shape silver NPs clearly reveals that there is a shape dependent interaction of the NPs.[42] Similarly, the relationship of the biological activity and size of the NPs is also noticeable. Chen *et al.* evaluated the antibacterial capability of different sized silver NPs deposited over graphene oxide and found that the smallest silver NPs exhibited higher antibacterial activity.[43]

Here, we report an approach for designing multifunctional TiO_2 nanofibers (NFs), photosensitized with varying sizes of Ag_2S nanoparticles (Ag_2S/TiO_2), and their effectiveness for the photo-reduction of Cr(VI) as well as photo-disinfection of the pathogenic bacteria, both Gram-positive and Gram-negative, under simulated solar light illumination. Overall the aim of this study is to investigate the size dependence of the Ag_2S NPs on the photosensitization of TiO_2 NFs and demonstrate their potential use in developing water remediation technologies using solar light.

Experimental

Material synthesis

Precursor NFs for TiO_2 were obtained by electrospinning of a mixture of 1.5 g polyvinylpyrrolidone (PVP, $M_w = 1\,300\,000$ g mol^{-1}), 4 g titanium(IV) *n*-butoxide (TNBT, 97%), 10 g ethanol and 4 g acetic acid. An electric field of 18 kV with a tip-to-collector distance of 18 cm was used. The collected precursor NF mat was left overnight for complete hydrolysis and then calcined at 500 °C for 2 h to obtain pure anatase TiO_2 NFs as shown in the Fig. 1(a) with a mean diameter of 195 nm. Ag_2S NPs of varying sizes were grown over TiO_2 NFs by reduction of Ag^+ to Ag followed by a sulfurization treatment. For this, 0.1 M NaOH was added to 0.01 M $AgNO_3$ solution (10 ml) until brown precipitates appeared. All brown precipitates were then dissolved by the addition of 1.0 M ammonia solution which is due to the formation of the complex, $[Ag(NH_3)_2]^+$, also known as the Tollens reagent. In this solution, 0.05 M dextrose solution (10 ml) and 20 mg of the TiO_2 NFs were added under constant stirring resulting in the formation of the Ag NPs. The size of the Ag NPs was controlled by varying the dipping times from 0.5–2.0 min. These NPs were subsequently sulfurized to Ag_2S by dipping in 25 ml of 0.01 M sulfur/acetonitrile solution at 60 °C for 10 min.[44] The synthesized composite Ag_2S/TiO_2 NFs were washed with acetonitrile and distilled water followed by oven drying at 60 °C. Selected samples were also subjected to a ultraviolet–ozone (UV–O_3) treatment for 2 h to induced excess surface Ti^{3+} chemical states which is expected to enhance the photo-reduction and photo-disinfection activity as reported earlier by the authors for the photodegradation of methylene blue (MB) dye.[45,46]

Photo-reduction of Cr(VI)

The photocatalytic activity of the Ag_2S/TiO_2 NFs was evaluated using carcinogenic Cr(VI) compound as a target pollutant in the aqueous media. The Cr(VI) stock solution (10 mg L^{-1}) was prepared by dissolving $K_2Cr_2O_7$ in deionized water. Then 20 mg of the Ag_2S/TiO_2 NFs was dispersed in 20 ml of the Cr(VI) solution and agitated in dark for 30 min to establish the adsorption–desorption equilibrium. The suspension was then irradiated with simulated solar light using 100 W xenon lamp. 1 ml of the suspension was taken out every 30 min and centrifuged. The Cr(VI) reduction was estimated spectrophotometrically ($\lambda = 540$ nm) by making their colored complex with diphenylcarbazide. Photo-reduction of Cr(VI) was evaluated at different pH values (3, 5, 7, 9) adjusted with 0.1 M HCl and 0.05 M NaOH solutions.

Photo-disinfection of *E. coli* and *S. aureus*

The antibacterial activity of the Ag_2S/TiO_2 NFs was studied *via* photochemical interaction of the NFs with the bacterial strains of Gram-negative *Escherichia coli* [ACCN, KJ880039] and Gram-positive *Staphylococcus aureus* [ACCN, KY635411] using the plate-count method. These strains were maintained in the LB broth and agar. Bacterial cultures were prepared by incubating their strains inoculated on the LB nutrient agar at 37 °C for 16–24 h under shaking and aerobic conditions. After this, the single colony of the bacterial strain was incubated in LB broth under standard conditions. Before the antibacterial assay, LB broth, nutrient agar, and all other apparatus such as L-rods, Petri plates, micro-tips, *etc.*, were sterilized by autoclaving at 120 °C for 30 min. Bacterial cultures were then centrifuged at 4000 rpm and washed with 0.9% saline solution. Bacterial pellets were then re-suspended and diluted with normal saline to prepare their suspension having 0.2 optical density (OD). The antibacterial activity was evaluated by mixing 5 mg of the NFs with 5 ml of the bacterial suspension in the

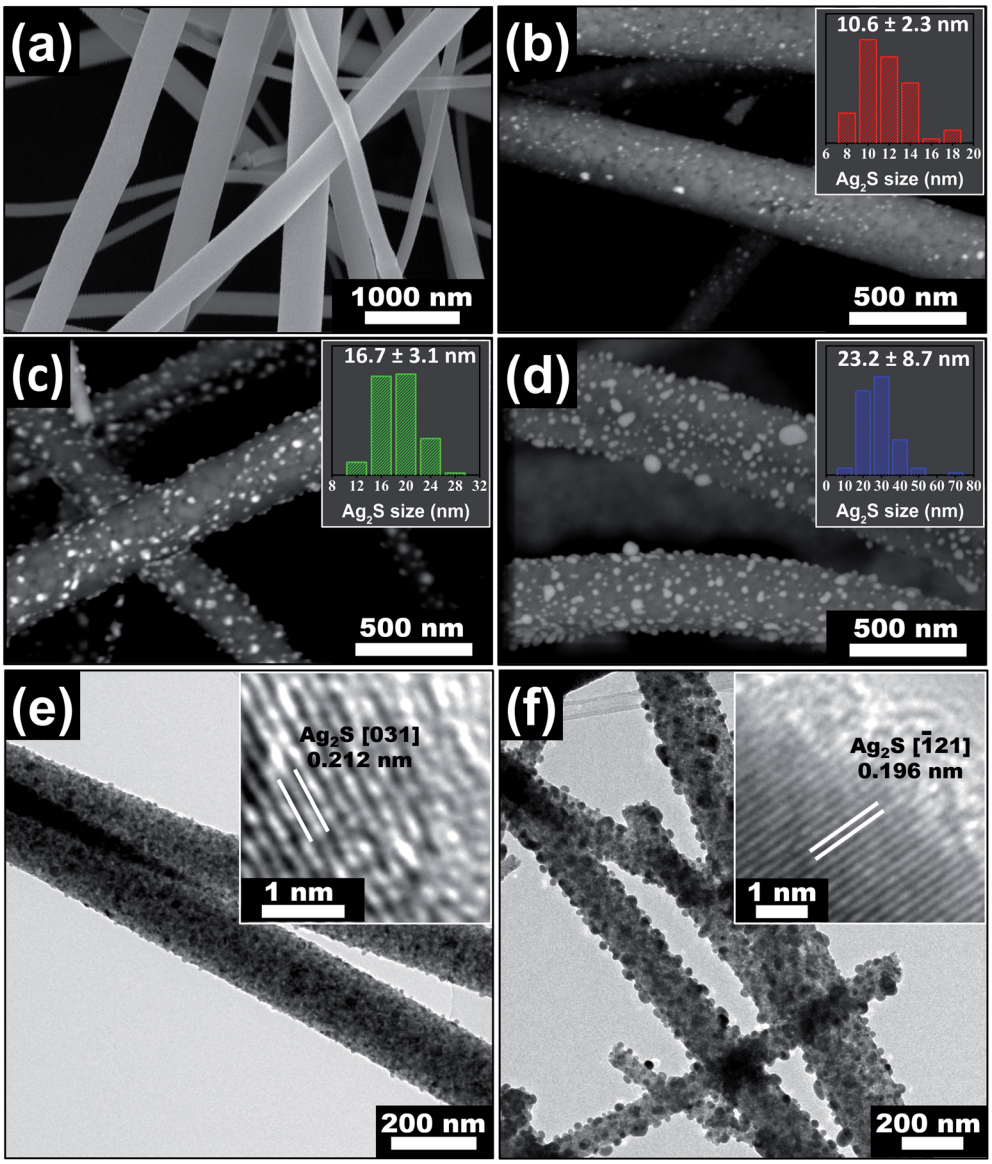

Fig. 1 SEM images of (a) electrospun TiO_2 nanofibers with mean diameter of 195 nm, (b) 11 nm Ag_2S/TiO_2, (c) 17 nm Ag_2S/TiO_2, and (d) 23 nm Ag_2S/TiO_2 nanofibers. TEM images of (e) 11 nm Ag_2S/TiO_2 and (f) 23 nm Ag_2S/TiO_2 nanofibers. The Ag_2S size distribution in the insets of (b–d) and HR-TEM images in the insets of (e and f) are reproduced from our previous work,[46] available under the Creative Commons Attribution 4.0 International Public License.

sterilized flask. The initial bacterial concentration was 1×10^8 CFU ml^{-1} for *E. coli* and 3×10^8 CFU ml^{-1} for *S. aureus* (CFU: colony forming units). A 100 W xenon lamp positioned at 15 cm from the reaction mixture was used for illumination under constant shaking. The irradiance, measured at the center of the reaction mixture with a power meter and Si photodiode sensor, was estimated to be ~10 mW cm^{-2}. The sterilized nutrient agar solution was poured in the Petri plates and allowed to solidify. At regular intervals of illumination, 100 μL of the treated bacterial suspension was withdrawn and diluted serially with normal saline to adjust the bacterial concentration (aliquots were diluted to 10^{-5} times in the present study) to ensure that the growing (reactivated) bacterial colonies were being counted accurately. Small quantity of this diluted bacterial suspension (100 μL) was spread onto the nutrient agar plates and the number of colonies were counted after incubating at 37 °C for 24 h. An average number of the colonies was obtained by repeating the above procedure three times for each NF sample. Bacterial suspension without NFs was also serially diluted and incubated on agar plates to count the number of colonies in the control sample. The bactericidal efficiency was calculated by the following equation.

$$\text{Bactericidal Efficiency } (\%) = \frac{N_{\text{control}} - N_{\text{sample}}}{N_{\text{control}}} \times 100$$

where N_{control} and N_{sample} denotes to the number of colonies counted in the control and the sample agar plates, respectively. Exactly the same procedure was also carried out in dark to explore the disinfection nature of the Ag_2S NPs only.

Results & discussion

Structure, morphology and chemistry of the materials

The SEM images of the fabricated Ag_2S/TiO_2 NFs in the Fig. 1(b–d) indicates successful deposition of the Ag NPs and their subsequent sulfurization to Ag_2S which was also confirmed previously by the X-ray photoelectron spectroscopy (XPS) and X-ray diffraction (XRD) studies.[46] The number-averaged size of the Ag_2S NPs is 11, 17, and 23 nm for the dipping times of 0.5, 1.0, and 2.0 min, respectively. These sizes were statistically measured from at least 100 NPs by measuring their areas and calculating the corresponding area-equivalent diameters assuming circular shape. The corresponding Ag_2S size distribution, shown in the insets of Fig. 1(b–d), characteristically shows log-normal distribution.[46] The weight percentages of the Ag_2S in the NFs was estimated by inductively coupled plasma optical emission spectroscopy (ICP-OES) by calibrating the emission intensity of Ag using a standard $AgNO_3$ salt solution of 1–10 ppm. The weight fractions were 4, 10, and 18% for 11, 17, and 23 nm Ag_2S/TiO_2 NFs, respectively. Fig. 1(e and f) shows the TEM images of the 11 nm and 23 nm Ag_2S/TiO_2 NFs, respectively, which also confirms the uniform distribution of the Ag_2S NPs over the TiO_2 NFs. The insets show the (031) lattice for the 11 nm Ag_2S/TiO_2 with d-spacing of 0.212 nm and (121) lattice for the 23 nm Ag_2S/TiO_2 with d-spacing of 0.196 nm, respectively.[46]

Fig. 2(a) shows the XRD scan of the pure TiO_2 and Ag_2S/TiO_2 samples where the Ag_2S lattices identified in the insets of Fig. 1(e and f) were clearly observed along with all other characteristics peaks for the monoclinic Ag_2S. No Ag peak was observed for any sample. Moreover, the formation of anatase TiO_2 is also confirmed from the observation of (101) and other characteristic peaks. Fig. 2(b) shows the XPS survey scan which confirms the presence of Ti and O in the pristine TiO_2 and furthermore Ag and S in the Ag_2S/TiO_2 NFs. The surface chemical states were characterized in detail using XPS and reported in our earlier work.[46] Fig. S1† shows the deconvoluted peaks of Ti 2p, O 1s, Ag 3d, and S 2p. Pure TiO_2 NFs showed 94.3% Ti^{4+} and 5.7% Ti^{3+} surface chemical states. The surface Ti^{3+} increases to 6.7% after deposition of 17 nm Ag_2S NPs with a shift to the higher binding energy indicative of the loss of the valence electron charge. Moreover, the surface UV–O_3 treatment further increases the Ti^{3+} to 8.2% indicating the removal of the lattice oxygen. The effect of these surface chemical changes *i.e.* the increased surface Ti^{3+} states and oxygen vacancies on the photocatalytic activity will be discussed later.

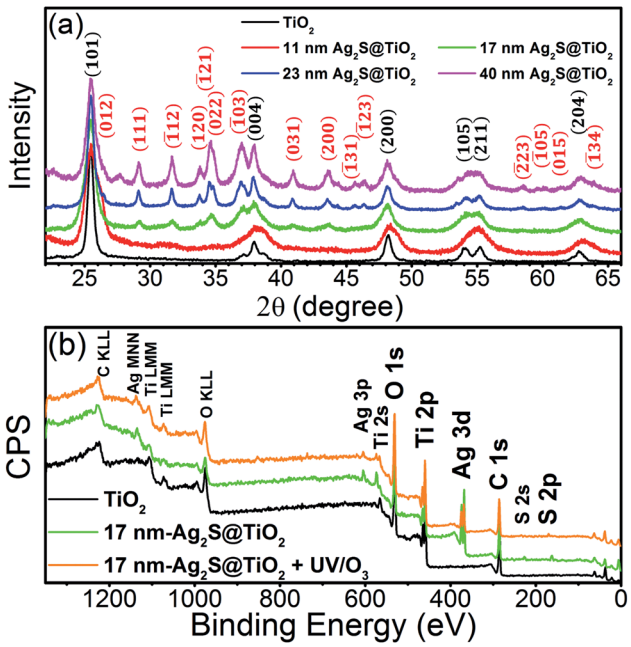

Fig. 2 (a) XRD scans of pristine TiO_2 and Ag_2S/TiO_2 NFs. (b) Full XPS survey scan of pure TiO_2, 17 nm Ag_2S/TiO_2 and 17 nm-Ag_2S/TiO_2 treated with UV–O_3. The figure is reproduced from our previous work,[46] available under the Creative Commons Attribution 4.0 International Public License.

The fabricated TiO_2 and Ag_2S/TiO_2 NFs are expected to be non-porous materials since no pore generating agent was used. This was confirmed by the adsorption–desorption isotherm shown in the Fig. S2(a)† which is typical for the multilayer formation in non-porous materials. The specific surface area of pure TiO_2 NFs and 17 nm Ag_2S/TiO_2 NFs was 7.1 and 6.6 $m^2\ g^{-1}$, respectively. Fig. S2(b)† shows the pore size distribution using the nonlocal density functional theory (NLDFT) method. The *t*-plot method was used to determine the micropores volume which was negligible. The collection of NFs as a mat during electrospinning does create the so-called macropores indicated by the high intake of nitrogen at higher relative pressures ($P/P_o > 0.8$).

Photo-reduction of Cr(VI)

The presence of heavy metal ions in water pose a serious threat to the living organisms. One such contamination is the Cr(VI) which is a common by-product of many industries and can be photocatalytically reduced to less toxic and less mobile Cr(III) state. Fig. 3(a) shows the influence of the pH on the photo-reduction of Cr(VI) over Ag_2S/TiO_2 NFs under simulated solar light irradiation. The amount of Cr(VI) reduced to Cr(III) at pH of 3, 5, 7, and 9 is 90, 67, 58, and 48%, respectively, for the 17 nm Ag_2S/TiO_2 NFs. In acidic medium, Cr(VI) exists as $HCrO_4^-$, CrO_4^{2-}, and $Cr_2O_7^{2-}$ anionic species.[47] Therefore, at lower pH, the surface of the Ag_2S/TiO_2 NFs are highly protonated which can easily accumulate the anionic species and hence facilitate the transfer of the photo-generated electrons towards the Cr(VI). At higher pH (>6.0), the surfaces of the NFs become negatively charged which tend to repel the anionic species and consequently decreases the photo-reduction kinetics. Moreover, the reduced Cr(III) is deposited on the surface of the NFs as $Cr(OH)_3$ at pH above 5, which is also responsible for the decreased photo-reduction efficiency.[48]

The size effect of the Ag_2S NPs on the photocatalytic reduction of Cr(VI) under simulated solar light at pH 3 was further investigated. The 17 nm Ag_2S/TiO_2 NFs showed 90% photocatalytic reduction of Cr(VI) with a pseudo-first order rate constant of 0.016 min^{-1}. In comparison, hollow spherical Ag–Ag_2S/TiO_2 composite particles under visible light irradiation were able to reduce only 36% Cr(VI) after 8 h irradiation.[40] This illustrates the significantly enhanced capacity of the TiO_2 NFs,

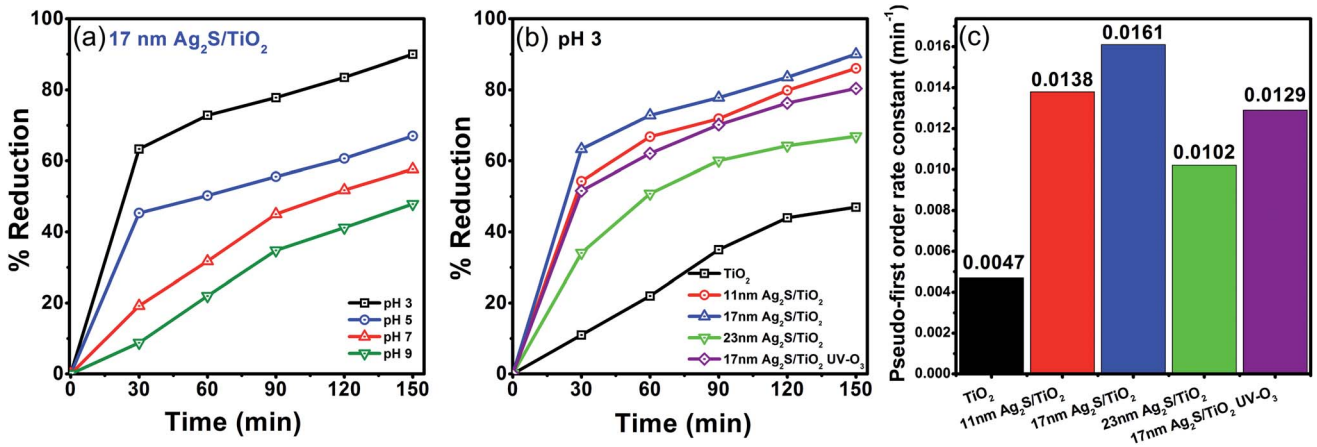

Fig. 3 (a) Photo-reduction of Cr(VI) at different pH values using 17 nm Ag_2S/TiO_2 nanofibers, (b) photo-reduction using variable sized Ag_2S/TiO_2 nanofibers at pH 3 compared to the pristine TiO_2 nanofibers, and (c) the corresponding pseudo-first order rate constants.

photosensitized with Ag_2S, reported here to reduce Cr(VI). The smaller (11 nm) and larger (23 nm) sized Ag_2S/TiO_2 NFs exhibited slower kinetics with pseudo-first order rate constants of 0.014 and 0.010 min^{-1}, respectively. This is in agreement with our findings on the role of Ag_2S NP size on the photo-degradation kinetics of methylene blue (MB) dye. Fig. S3† shows the enhanced visible-light harvesting capability, reduced bandgaps, and diminished photoluminescence signal when TiO_2 NFs are photosensitized by Ag_2S NPs. This is attributed to the efficient charge separation, charge transfer, and reduced electron–hole recombination. The UV–O_3 surface treatment of Ag_2S/TiO_2 NFs generates excess Ti^{3+} states which further facilitates the charge separation process[46] (Fig. S3†) but the photo-reduction of Cr(VI) was hindered as shown by the reduction of the rate constant to 0.013 min^{-1} for the 17 nm Ag_2S/TiO_2 NFs. As reported in the XPS results previously,[46] some of the Ag_2S get oxidized after UV–O_3 treatment and produces Ag_2SO_4 which is partially soluble in water. Introduction of the sulfate ions in the solution probably interferes with the sorption of the Cr(VI) over the NFs and, thus, suppresses the overall photo-reduction process. Thus, excess Ti^{3+} was beneficial for photo-degradation of methylene blue (MB) dye,[46] but not for the photo-reduction of Cr(VI) here. However, as shown below, the excess Ti^{3+} chemical states enhances the antibacterial performance of these materials.

Photo-disinfection efficiency in dark

The photocatalytic disinfection efficiencies of the Ag_2S/TiO_2 NFs were investigated on Gram-negative and Gram-positive bacteria. Fig. 4(a and b) shows the bactericidal efficiencies of both strains for 3 h in dark conditions. TiO_2 NFs alone have negligible effect on the survival of both strains, however, Ag_2S loading on the TiO_2 NFs significantly enhances the bactericidal efficiencies. Furthermore, UV–O_3 treatment of the 11 nm Ag_2S/TiO_2 NFs effectively inactivates almost all the bacteria. Smallest sized and spherical shaped Ag_2S NPs loading showed superior antibacterial activities compared to the larger and relatively irregular shaped Ag_2S NPs. These results are in good agreement with the reported studies on the effect of size and shape of Ag NPs on the bacterial viabilities.[43,49]

The bacterial decay in dark is an interesting observation and is due to Ag_2S only since TiO_2 has negligible effect. Recently, uncapped Ag_2S NPs showed antibacterial effect, calculated by the disc diffusion method, towards Gram-positive *S. aureus* and Gram-negative *E. coli*, with recorded inhibition zones of 15.81 and 10.34 mm, respectively.[50] Similarly, Ag_2S and Cu-doped Ag_2S NPs, prepared by the simple co-precipitation method, showed antibacterial activity both in dark and visible-light irradiation against *E. faecalis* and *S. aureus*.[51] However, the mechanisms of the antibacterial activity for silver containing compounds especially Ag_2S are not yet clearly known due to very limited work. Ag_2S exhibits very low solubility and reactivity and, thus, the mechanism for their cytotoxicity might be different than the widely accepted mechanism reported for ionic silver (Ag^+) and Ag NPs.[52] Wang *et al.* reported for the first time the toxic effects of Ag_2S NPs in plant tissues of cowpea (*Vigna unguiculata*) and wheat (*Triticum aestivum*) by direct uptake.[53] Using K-edge X-ray absorption near edge structure (XANES) and k^2-weighted extended X-ray absorption fine structure (EXAFS) they showed that almost all the Ag in the roots is stored as Ag_2S and is not sourced from the dissolved Ag in the solution. Pang *et al.* reported negligible inactivation efficiency against *E. coli* in dark using Ag_2S/Ag heterodimers probably due to much larger Ag size of 50–75 nm.[39] Ag_2S/Ag hetero-nanostructures and Ag NPs showed minimum inhibitory concentration (MIC) of 8 μg ml^{-1} against *E. coli* but Ag_2S NPs alone showed MIC of 32 μg ml^{-1} and it was concluded that the major contribution to the antibacterial activity in dark is coming from Ag.[54] In contrast, Ag_2S NPs over TiO_2 in the present study shows appreciable antibacterial activity which is promising but warrants further work to investigate the mechanism of the Ag_2S cytotoxicity.

Photo-disinfection efficiency under simulated sunlight

Next, the inactivation of bacteria by Ag_2S/TiO_2 NFs under simulated solar light illumination was studied. As shown in the Fig. 4(c and d), for 11 nm Ag_2S/TiO_2 NFs, the bactericidal efficiency increased rapidly to 100% and 90.6% against *E. coli* and *S. aureus* after 1 h of irradiation, respectively, whereas, only 50%

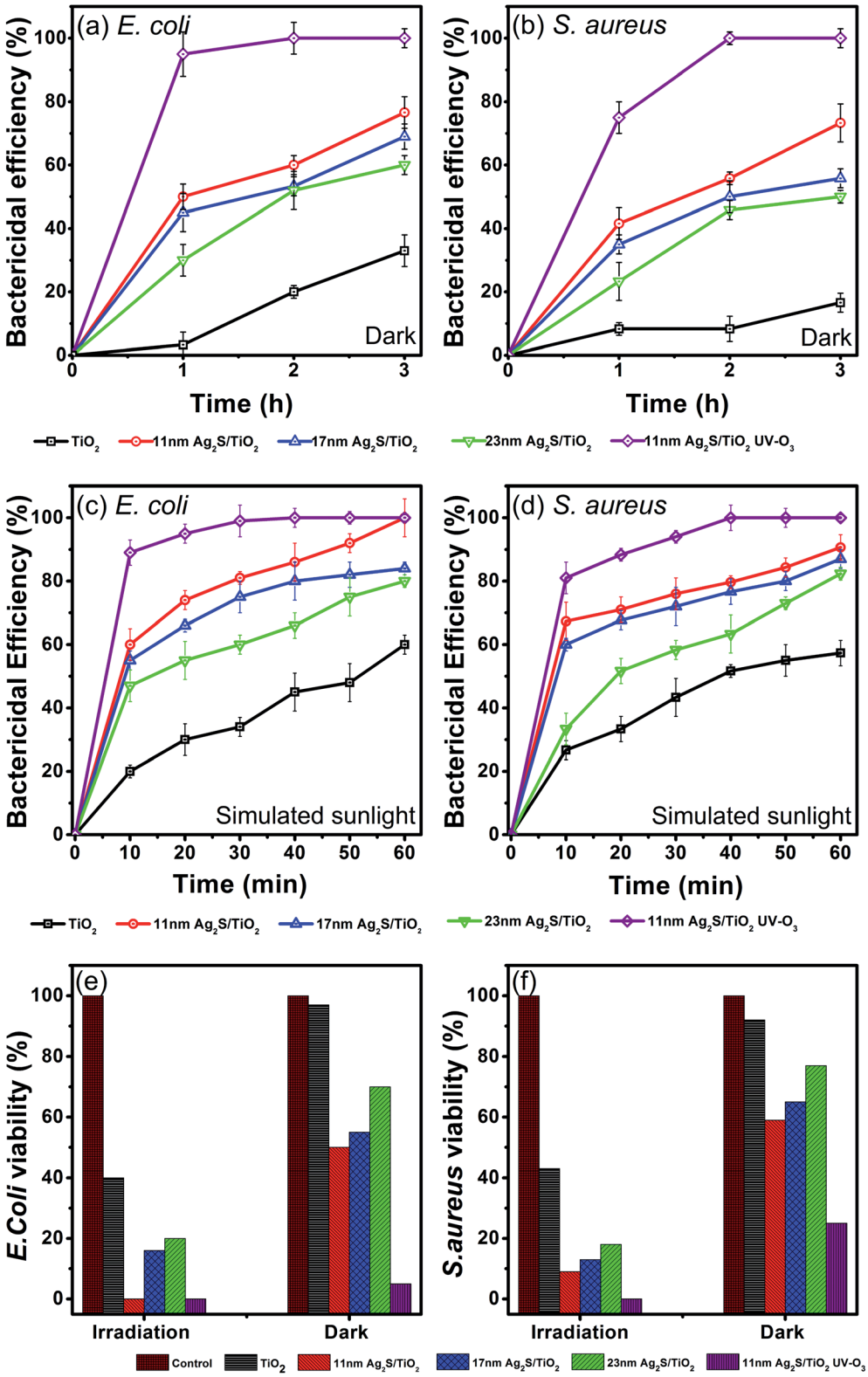

Fig. 4 (a and b) Bactericidal efficiency of *E. coli* and *S. aureus* in dark and (c and d) under simulated solar light irradiation, respectively. Comparison of the bacterial viabilities of (e) *E. coli* and (f) *S. aureus* after treatment with pristine TiO_2 and Ag_2S/TiO_2 nanofibers. Error bars represent standard deviations from triplicate experiments.

E. coli and 41% *S. aureus* were found to be inactivated under dark. UV–O_3 treatment on the 11 nm Ag_2S/TiO_2 NFs significantly enhanced the antibacterial activity with 89% *E. coli* and 81% *S. aureus* being inactivated in just 10 min of the irradiation. This is probably due to the synergistic effect of Ag^+ ions, originating from the dissolution of the Ag_2SO_4 formed by UV–O_3

treatment. The viabilities of the bacteria significantly decline under the solar light irradiation compared to the dark conditions. Moreover, the initial disinfection effectiveness against *E. coli* is higher than *S. aureus* and is discussed below.

The Ag_2S/TiO_2 NFs in the present study, when irradiated under simulated sunlight, produces hydroxyl radicals ($^{\bullet}OH$) by the reaction of the positively charged hole (h^+) with the hydroxide ion (OH^-).[46] The hydroxyl radicals are known to destruct the bacterial cell of Gram-positive and Gram-negative bacteria by breaking the covalent bonds in the peptidoglycan layer.[55] Moreover, the cell wall in Gram-positive and Gram-negative is structurally distinct and can initially respond differently to the toxic effects as seen in the Fig. 4(c and d) for the bactericidal efficiency after 10 min. Cell wall in Gram-negative consists of a membrane of lipopolysaccharide covered by a thin layer of peptidoglycan (~few nm). Cell wall in Gram-positive consists of much thicker peptidoglycan layer (~10s of nm). Thus, the initial response at 10 min to the effect of hydroxyl radicals and photo-disinfection of Ag_2S/TiO_2 NFs is slow in Gram-positive *S. aureus versus* Gram-negative *E. coli*. However, after 60 min both bacterial strains show similar inactivation. Similar trend was observed in dark which suggests that the effectiveness of Ag_2S NPs is indeed controlled by the nature of the target bacterial cell wall. Another contributing factor is the surface charge on the TiO_2 and the bacterial strains. TiO_2 is positively charged in acidic conditions (<pH 6).[56] Cell walls of most bacterial strains are known to possess negative surface charge due to the teichoic acids in Gram-positive and lipopolysaccharides & lipoproteins in Gram-negative bacteria.[30] Thus, the electrostatic bacterial adhesion to TiO_2 NFs is promoted for both Gram-positive and Gram-negative strains. Surface charge on the *S. aureus* (0.086 coulomb/10^9 CFU) is reported to be less than *E. coli* (0.129 coulomb/10^9 CFU) with corresponding electrostatically adhered TiO_2 amount of 0.61 and 1.88 g/10^9 CFU, respectively. These observations are in good agreement with the initially higher antibacterial activity against *E. coli versus S. aureus* reported here.

Morphological changes in *E. coli* cell wall

The morphological changes in the cell wall of *E. coli* treated with Ag_2S/TiO_2 NFs under simulated sunlight was observed in SEM (operated under STEM mode). Fig. 5(a) shows the characteristic rod-shaped morphology of the untreated *E. coli* (length ~2 μm, diameter ~0.5 μm) with an intact cell wall and interior. Fig. 5(b) shows the significant shape changes and rupturing of the cell wall after exposure to simulated solar light in the presence of 11 nm Ag_2S/TiO_2 NFs. The image contrast suggests that the outer membrane of the *E. coli* is disrupted at several locations in the same cell with leakage of the intracellular components. In a related study using Ag_2S/Ag heterodimers, tested for bacterial disinfection using similar methods, it was shown by inductively coupled plasma mass spectroscopy (ICP-MS) that the Ag^+ ion concentration in the *E. coli* suspensions was extremely low (~75 parts per billion) and energy dispersive X-ray spectroscopy (EDX) confirmed no change in the molar ratios of Ag : S for the catalysts before and after the tests. These findings confirmed that Ag^+ ions played no part in the bactericidal processes.[39] The cytotoxic action is, thus, initiated by the cell wall damage in the presence of Ag_2S/TiO_2 NFs followed by intracellular leakage. This cell wall damage could be due to the presence of hydroxyl radicals generated by Ag_2S/TiO_2 NFs[46] as well as due to the disinfectant nature of the pristine Ag_2S as reported here in dark. This later effect needs to be investigated mechanistically in the follow-up studies.

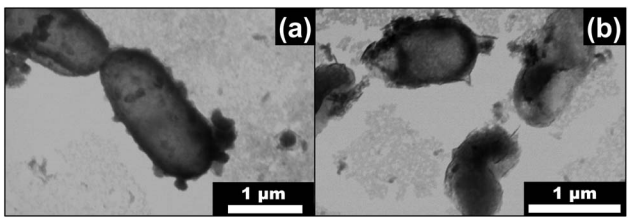

Fig. 5 The STEM images of the (a) untreated rod-shaped *E. coli* bacteria with a length of ~2 μm and width of ~0.5 μm, and the corresponding (b) treated *E. coli* bacteria showing significant shape changes and rupturing of the cell walls after exposure to simulated solar light irradiation in the presence of 11 nm Ag_2S/TiO_2 NFs.

Stability and the proposed photocatalytic mechanism

The stability of the UV–O_3 treated Ag_2S/TiO_2 NFs for the photocatalytic inactivation of *E. coli* was investigated for five cycles and the results are shown in the Fig. 6(a). After each cycle, the sample was washed with ethanol and subsequently with normal saline to decompose and remove all the captured bacteria. As it can be seen, the bactericidal efficiency of the bacteria slightly decreased initially probably due to the initial material loss during handling. Nevertheless, it becomes relatively stable after the second cycle.

The proposed photocatalytic mechanism in Ag_2S/TiO_2 NFs for the reduction of Cr(VI) can be explained in the Fig. 6(b). Owing to the small bandgap of Ag_2S ($E_g \sim 1$ eV), the valence band (VB) electrons are easily excited to the conduction band (CB) under visible light illumination. The photo-generated electrons transfer from CB of Ag_2S to the CB of TiO_2 which effectively inhibits the e^-–h^+ recombination. This effective charge separation facilitate the transfer of photo-generated electrons to Cr(VI) to reduce it to Cr(III), meanwhile the holes oxidize water and produce oxygen.[57] The reactions can be presented as:

$$Ag_2S/TiO_2 + h\nu \rightarrow Ag_2S/TiO_2 + e^- + h^+$$

$$Cr_2O_7^{2-} + 14H^+ + 6e^- \rightarrow 2Cr^{3+} + 7H_2O$$

$$2H_2O + 4h^+ \rightarrow O_2 + 4H^+$$

Similarly, the underlying mechanism for the photocatalytic inactivation of bacteria after treatment with Ag_2S/TiO_2 NFs under irradiation can be explained. In addition, the Ti^{3+} states introduced after UV–O_3 treatment further promotes the lifetime of the charges.[46] The photo-generated electrons and holes react with O_2 and H_2O to produce the reactive oxygen species (ROS) such as peroxide ($O_2^{-\bullet}$) and hydroxide ($^{\bullet}OH$) radicals. These ROS diffuse

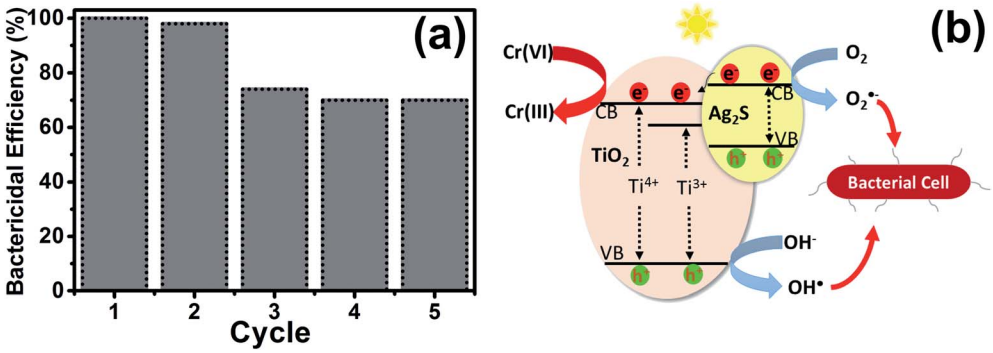

Fig. 6 (a) Bactericidal efficiency against *E. coli* (10^8 CFU ml^{-1}) in the presence of 11 nm Ag_2S/TiO_2 NFs treated with UV–O_3 over five cycles under simulated solar light illumination. (b) Schematic of the proposed mechanisms for the photo-reduction of Cr(VI) and photo-disinfection of bacteria by Ag_2S/TiO_2 NFs.

in the cell wall of bacteria and react with the cell membrane and DNA leading to death of the bacteria.[58] As stated above, Ag^+ and sulfate SO_4^{2-} ions introduced after UV–O_3 treatment, though not beneficial for the reduction of Cr(VI), further accelerate the bactericidal activity due to the synergistic effect from Ag^+.

Conclusions

In summary, TiO_2 NFs were photosensitized by Ag_2S NPs with mean sizes of 11, 17, and 23 nm, for potential applications in water remediation by reducing heavy metal ions and inactivating bacteria under simulated solar light irradiation. The 17 nm Ag_2S/TiO_2 NFs showed superior photocatalytic reduction of Cr(VI) at pH 3. Enhanced photocatalytic activity is attributed to the efficient charge separation and transfer and reduced electron–hole recombination. Furthermore, the 11 nm Ag_2S/TiO_2 NFs treated with UV–O_3 to induce excess Ti^{3+} chemical states showed excellent photocatalytic disinfection of both Gram-negative *E. coli* and Gram-positive *S. aureus* bacterial strains. The enhanced cytotoxicity is attributed to several factors such as disinfectant nature of the pristine Ag_2S, role of hydroxyl radicals, good adhesion between positively charged TiO_2 and negatively charged bacteria, and the synergistic effect of Ag^+ (only for UV–O_3 treated sample). These multifunctional composite nanofibers can potentially be used for water remediation under solar light.

Conflicts of interest

There are no conflicts to declare.

Acknowledgements

We acknowledge Dr Murtaza Saleem, Sr Research Scientist in the Central Labs of the Syed Babar Ali School of Science and Engineering, LUMS, for help with the scanning electron microscopy (SEM) and Dr Nasir Mahmood, University of Wollongong, for assistance in the X-ray photoelectron spectroscopy (XPS). We are also thankful to Mr Muhammad Usman Ghafoor for helping with the simulated solar light irradiation setup.

References

1 S. Pigeot-Rémy, F. Simonet, E. Errazuriz-Cerda, J. C. Lazzaroni, D. Atlan and C. Guillard, *Appl. Catal., B*, 2011, **104**, 390–398.
2 M. A. Shannon, P. W. Bohn, M. Elimelech, J. G. Georgiadis, B. J. Marñas and A. M. Mayes, *Nature*, 2008, **452**, 301–310.
3 G. Xiao, X. Zhang, W. Zhang, S. Zhang, H. Su and T. Tan, *Appl. Catal., B*, 2015, **170–171**, 255–262.
4 S. W. Krasner, H. S. Weinberg, S. D. Richardson, S. J. Pastor, R. Chinn, M. J. Sclimenti, G. D. Onstad and A. D. Thruston, *Environ. Sci. Technol.*, 2006, **40**, 7175–7185.
5 S. E. Bailey, T. J. Olin, R. M. Bricka and D. D. Adrian, *Water Res.*, 1999, **33**, 2469–2479.
6 Q. Li, S. Mahendra, D. Y. Lyon, L. Brunet, M. V. Liga, D. Li and P. J. J. Alvarez, *Water Res.*, 2008, **42**, 4591–4602.
7 Y. C. Zhang, J. Li and H. Y. Xu, *Appl. Catal., B*, 2012, **123–124**, 18–26.
8 N. Hsu, S. Wang, Y. Lin, G. Sheng and J. Lee, *Environ. Sci. Technol.*, 2009, **43**, 8801–8806.
9 M. Yadav and Q. Xu, *Chem. Commun.*, 2013, **49**, 3327.
10 G. T. Fu, X. Jiang, R. Wu, S. H. Wei, D. M. Sun, Y. W. Tang, T. H. Lu and Y. Chen, *ACS Appl. Mater. Interfaces*, 2014, **6**, 22790–22795.
11 Z. W. Wang, Z. Y. Wang, D. M. Wang and M. Chen, *RSC Adv.*, 2016, **6**, 12286–12289.
12 A. Kumar, C. Guo, G. Sharma, D. Pathania, M. Naushad, S. Kalia and P. Dhiman, *RSC Adv.*, 2016, **6**, 13251–13263.
13 B. Vellaichamy and P. Periakaruppan, *RSC Adv.*, 2016, **6**, 57380–57388.
14 X. Xin, J. Lang, T. Wang, Y. Su, Y. Zhao and X. Wang, *Appl. Catal., B*, 2016, **181**, 197–209.
15 S. Y. Chai, Y. J. Kim, M. H. Jung, A. K. Chakraborty, D. Jung and W. I. Lee, *J. Catal.*, 2009, **262**, 144–149.
16 W. Liu, M. Wang, C. Xu and S. Chen, *Chem. Eng. J.*, 2012, **209**, 386–393.
17 A. Fujishima and K. Honda, *Nature*, 1972, **238**, 37–38.
18 M. Ni, M. K. H. Leung, D. Y. C. Leung and K. Sumathy, *Renewable Sustainable Energy Rev.*, 2007, **11**, 401–425.
19 H. Abdullah, D. H. Kuo and Y. H. Chen, *J. Mater. Sci.*, 2016, **51**, 8209–8223.

20 Y. Li, L. Zhang, W. Wu, P. Dai, X. Yu, M. Wu and G. Li, *Nanoscale Res. Lett.*, 2014, **9**, 270–275.
21 W. Choi, A. Termin and M. R. Hoffmann, *J. Phys. Chem.*, 1994, **98**, 13669–13679.
22 Y. Cong, J. Zhang, F. Chen and M. Anpo, *J. Phys. Chem. C*, 2007, **111**, 6976–6982.
23 A. Yousef, R. M. Brooks, M. M. El-Halwany, N. A. M. Barakat, M. H. EL-Newehy and H. Y. Kim, *Chem. Eng. Process. Process Intensif.*, 2015, **95**, 202–207.
24 G. Marotta, M. G. Lobello, C. Anselmi, G. Barozzino Consiglio, M. Calamante, A. Mordini, M. Pastore and F. De Angelis, *ChemPhysChem*, 2014, **15**, 1116–1125.
25 P. Chowdhury, J. Moreira, H. Gomaa and A. K. Ray, *Ind. Eng. Chem. Res.*, 2012, **51**, 4523–4532.
26 P. Zhang, C. Shao, Z. Zhang, M. Zhang, J. Mu, Z. Guo, Y. Sun and Y. Liu, *J. Mater. Chem.*, 2011, **21**, 17746.
27 T. Zhu, C. K. Nuo Peh, M. Hong and G. W. Ho, *Chem.–Eur. J.*, 2014, **20**, 11505–11510.
28 L. Deng, H. Liu, X. Gao, X. Su and Z. Zhu, *Ceram. Int.*, 2015, **42**, 3808–3815.
29 M. Gholami, M. Qorbani, O. Moradlou, N. Naseri and A. Z. Moshfegh, *RSC Adv.*, 2014, **4**, 7838.
30 S. P. Tallósy, L. Janovák, E. Nagy, Á. Deák, Á. Juhász, E. Csapó, N. Buzás and I. Dékány, *Appl. Surf. Sci.*, 2016, **371**, 139–150.
31 B. Liu, L. Mu, B. Han, J. Zhang and H. Shi, *Appl. Surf. Sci.*, 2017, **396**, 1596–1603.
32 R. Michal, E. Dworniczek, M. Caplovicova, O. Monfort, P. Lianos, L. Caplovic and G. Plesch, *Appl. Surf. Sci.*, 2016, **371**, 538–546.
33 X. Zheng, Z. Shen, C. Cheng, L. Shi, R. Cheng and J. Dong, *RSC Adv.*, 2017, **7**, 52172–52179.
34 J. Li, D. Ren, Z. Wu, C. Huang, H. Yang, Y. Chen and H. Yu, *RSC Adv.*, 2017, **7**, 55131–55140.
35 J. S. Kim, E. Kuk, K. N. Yu, J. H. Kim, S. J. Park, H. J. Lee, S. H. Kim, Y. K. Park, Y. H. Park, C. Y. Hwang, Y. K. Kim, Y. S. Lee, D. H. Jeong and M. H. Cho, *Nanomed. Nanotechnol. Biol. Med.*, 2007, **3**, 95–101.
36 C. Tang, H. Bai, L. Liu, X. Zan, P. Gao, D. D. Sun and W. Yan, *Appl. Catal., B*, 2016, **196**, 57–67.
37 E. Albert, P. A. Albouy, A. Ayral, P. Basa, G. Csík, N. Nagy, S. Roualdès, V. Rouessac, G. Sáfrán, Á. Suhajda, Z. Zolnai and Z. Hórvölgyi, *RSC Adv.*, 2015, **5**, 59070–59081.
38 D. Wei, F. Tian, Z. Lu, H. Yang and R. Chen, *RSC Adv.*, 2016, **6**, 52264–52270.
39 M. Pang, J. Hu and H. C. Zeng, *J. Am. Chem. Soc.*, 2010, **132**, 10771–10785.
40 D. Zhang, G. Xu and F. Chen, *Appl. Surf. Sci.*, 2015, **351**, 962–968.
41 S. Agnihotri, S. Mukherji and S. Mukherji, *RSC Adv.*, 2014, **4**, 3974–3983.
42 S. Pal, Y. K. Tak and J. M. Song, *J. Biol. Chem.*, 2015, **290**, 1712–1720.
43 X. Chen, X. Huang, C. Zheng, Y. Liu, T. Xu and J. Liu, *J. Mater. Chem. B*, 2015, **3**, 7020–7029.
44 X. Liu, Z. Liu, J. Lu, X. Wu and W. Chu, *J. Colloid Interface Sci.*, 2014, **413**, 17–23.
45 S. Dilpazir, M. Usman, S. Rasul and S. N. Arshad, *RSC Adv.*, 2016, **6**, 14751–14755.
46 S. Ghafoor, S. Ata, N. Mahmood and S. N. Arshad, *Sci. Rep.*, 2017, **7**(255), 1–10.
47 J. Su, Y. Zhang, S. Xu, S. Wang, H. Ding, S. Pan, G. Wang, G. Li and H. Zhao, *Nanoscale*, 2014, **6**, 5181.
48 M. Shirzad-Siboni, M. Farrokhi, R. Darvishi Cheshmeh Soltani, A. Khataee and S. Tajassosi, *Ind. Eng. Chem. Res.*, 2014, **53**, 1079–1087.
49 A. GhavamiNejad, A. Rajan Unnithan, A. Ramachandra Kurup Sasikala, M. Samarikhalaj, R. G. Thomas, Y. Y. Jeong, S. Nasseri, P. Murugesan, D. Wu, C. Hee Park and C. S. Kim, *ACS Appl. Mater. Interfaces*, 2015, **7**, 12176–12183.
50 D. Ayodhya and G. Veerabhadram, *J. Photochem. Photobiol., B*, 2016, **157**, 57–69.
51 A. Fakhri, M. Pourmand, R. Khakpour and S. Behrouz, *J. Photochem. Photobiol., B*, 2015, **149**, 78–83.
52 J. Y. Maillard and P. Hartemann, *Crit. Rev. Microbiol.*, 2013, **39**, 373–383.
53 P. Wang, N. W. Menzies, E. Lombi, R. Sekine, F. P. C. Blamey, M. C. Hernandez-Soriano, M. Cheng, P. Kappen, W. J. G. M. Peijnenburg, C. Tang and P. M. Kopittke, *Nanotoxicology*, 2015, **9**, 1041–1049.
54 X. Ma, Y. Zhao, X. Jiang, W. Liu, S. Liu and Z. Tang, *ChemPhysChem*, 2012, **13**, 2531–2535.
55 L. Ge, G. Na, S. Zhang, K. Li, P. Zhang, H. Ren and Z. Yao, *Sci. Total Environ.*, 2015, **527–528**, 12–17.
56 T. Preocanin and N. Kallay, *Croat. Chem. Acta*, 2006, **79**, 95–106.
57 H. Chu, W. Lei, X. Liu, J. Li, W. Zheng, G. Zhu, C. Li, L. Pan and C. Sun, *Appl. Catal., A*, 2016, **521**, 19–25.
58 W. S. Lee, Y.-S. Park and Y.-K. Cho, *Analyst*, 2015, **140**, 616–622.

